The ISME Journal (2018) 12, 495–507

www.nature.com/ismej

ORIGINAL ARTICLE

Electron carriers in microbial sulfate reduction inferred from experimental and environmental sulfur isotope fractionations

Christine B Wenk[1], Boswell A Wing[2] and Itay Halevy[1]
[1]Department of Earth and Planetary Sciences, Weizmann Institute of Science, Rehovot, Israel and
[2]Department of Geological Sciences, University of Colorado, Boulder, CO, USA

Dissimilatory sulfate reduction (DSR) has been a key process influencing the global carbon cycle, atmospheric composition and climate for much of Earth's history, yet the energy metabolism of sulfate-reducing microbes remains poorly understood. Many organisms, particularly sulfate reducers, live in low-energy environments and metabolize at very low rates, requiring specific physiological adaptations. We identify one such potential adaptation—the electron carriers selected for survival under energy-limited conditions. Employing a quantitative biochemical-isotopic model, we find that the large S isotope fractionations (>55‰) observed in a wide range of natural environments and culture experiments at low respiration rates are only possible when the standard-state Gibbs free energy ($\Delta G'°$) of all steps during DSR is more positive than −10 kJ mol^{-1}. This implies that at low respiration rates, only electron carriers with modestly negative reduction potentials are involved, such as menaquinone, rubredoxin, rubrerythrin or some flavodoxins. Furthermore, the constraints from S isotope fractionation imply that ferredoxins with a strongly negative reduction potential cannot be the direct electron donor to S intermediates at low respiration rates. Although most sulfate reducers have the genetic potential to express a variety of electron carriers, our results suggest that a key physiological adaptation of sulfate reducers to low-energy environments is to use electron carriers with modestly negative reduction potentials.
The ISME Journal (2018) **12,** 495–507; doi:10.1038/ismej.2017.185; published online 31 October 2017

Introduction

A large part of Earth's microbiome exists under energy limitation (Whitman *et al.*, 1998; Kallmeyer *et al.*, 2012; Lever *et al.*, 2015; Lau *et al.*, 2016) and metabolizes at rates 10^4 to 10^6 times slower than organisms in culture (Hoehler and Jørgensen, 2013). As the subsurface continental and seabed environments in which these organisms persist are largely inaccessible to direct experimentation, their physiology and biochemistry in their natural habitats are unresolved. How do these organisms maintain basic cell functions, such as growth and division, under such extreme energy limitation?

Sulfate-reducing bacteria and archaea, which are responsible for about half of the organic matter respiration in marine sediments (Jørgensen, 1982), are among the keystone organisms in many low-energy environments (Edwards *et al.*, 2005; Jørgensen and D'Hondt, 2006; Orsi *et al.*, 2016). They metabolize at extremely low rates (Hoehler and Jørgensen, 2013; Bowles *et al.*, 2014; Jørgensen and Marshall, 2016), which must require physiological adaptations such as increased efficiency of substrate uptake (Lever *et al.*, 2015; Jørgensen and Marshall, 2016). The exact adaptive tactics that enable their strategy of persistence, however, remain unknown. In particular, it is unclear how the varied spectrum of electron carriers in sulfate-reducing organisms (SROs) might support energy conservation under energy-limited natural conditions.

Single-cell genomic studies show that most sulfate reducers have the genetic potential to express a variety of electron carriers, such as menaquinones, and all of them have genes encoding for ferredoxin (Pereira *et al.*, 2011). High potential electron carriers like ferredoxins are often abundant in environmental metagenomes from subsurface environments that host SROs (Orsi *et al.*, 2013; Keller *et al.*, 2015; Lau *et al.*, 2016; Oberding and Gieg, 2016; Wu *et al.*, 2016), whereas metatranscriptome studies of S-driven deep subsurface microbial ecosystems have also identified gene transcripts encoding for small proteins with low redox potential like rubredoxin and rubrerythrin expressed by SROs (Lau *et al.*, 2016; Orsi *et al.*, 2016). The physiological role of those

Correspondence: CB Wenk or I Halevy, Department of Earth and Planetary Sciences, Weizmann Institute of Science, Rehovot, Israel.
E-mail: chwenk@gmail.com or itay.halevy@weizmann.ac.il
Received 20 April 2017; revised 26 August 2017; accepted 24 September 2017; published online 31 October 2017

proteins remains unclear. However, the mere presence of rubredoxin- and rubrerythrin-encoding gene transcripts in these anoxic environments is puzzling, as both proteins are proposed to function as part of an oxidative stress response system in laboratory cultures of sulfate-reducing bacteria (Lumppio *et al.*, 2001).

We investigated this apparent ecological inconsistency with a systems biochemical model of S isotope fractionation during dissimilatory sulfate reduction. We show that the reduction potential of the intracellular electron carriers for this metabolic pathway controls the magnitude of the S isotope fractionation that it produces. In turn, this allows us to connect S isotope fractionations and environmental electron donors observed in subsurface environments to the potential physiological roles of electron carriers in SROs. The widespread occurrence of large S isotope fractionations in many energy-limited environments suggests that the ability to use electron carriers with very modest reduction potentials is of general importance and a key adaptation of sulfate reducers living in energy-limited environments.

Electron carrier identity is a critical component of the energy metabolism of SROs

SROs use a respiratory mechanism with sulfate (SO_4^{2-}) as the terminal electron acceptor. The dissimilatory reduction of SO_4^{2-} (DSR) is a multistep reaction (Figure 1), where SO_4^{2-} is first symported into the cell, activated with adenosine triphosphate (ATP) to form adenosine 5′phosphosulfate (APS), which is then reduced to sulfite (SO_3^{2-}) and ultimately to sulfide (H_2S). A comparative genomic analysis shows conservation of genes encoding for the sulfur metabolic enzymes (sulfate transporters, sulfate adenylyl transferase, APS reductase and dissimilatory sulfite reductase (DsrAB)) for the membrane-bound Qmo and Dsr complexes, as well as for ferredoxin across 25 sequenced SROs (Figure 1) (Pereira *et al.*, 2011).

Although the physiological role of most of the conserved key enzymes in SROs has been resolved (Figure 1), their interaction with electron carriers remains uncertain. In addition to ferredoxin, menaquinone is present in most sulfate reducers (Collins and Widdel, 1986; Tindall *et al.*, 1989). As menaquinones are membrane-bound, they can be directly involved in energy conservation by contributing to a transmembrane proton gradient. As a result, recent biochemical work has focused on finding a direct physiological role of menaquinone and the omnipresent ferredoxin in DSR (Ramos *et al.*, 2012; Keller *et al.*, 2014; Price *et al.*, 2014a; Duarte *et al.*, 2016).

APS reduction, for example, is catalyzed by APS reductase, which receives electrons through the membrane-bound quinone-interacting oxidoreductase (Qmo) complex (Fritz *et al.*, 2002; Ramos *et al.*, 2012; Duarte *et al.*, 2016). Although it is generally assumed that menaquinone oxidation releases electrons to the membrane-bound QmoC subunit, this may be thermodynamically unfavorable because of the similar potentials of APS reduction (E'° APS/AMP+HSO_3^- = −65 mV) and menaquinone reduction (E'° MK/MKH_2 = −74 mV) at standard conditions (Ramos *et al.*, 2012). Hence, ferredoxin, with a more negative standard-state reduction potential (−398 mV; Ramos *et al.*, 2012), has been proposed to be involved in the reduction of APS through an electron confurcation scheme (Ramos *et al.*, 2012; Keller *et al.*, 2014; Price *et al.*, 2014b; Rabus *et al.*, 2015).

The direct electron donors during sulfite reduction are even less well known (Figure 1). Two electrons are transferred to the catalytic site of DsrAB through an unidentified electron carrier, reducing SO_3^{2-} to an enzyme-bound S^{II} intermediate (Santos *et al.*, 2015). DsrC, a small soluble protein with a C-terminal arm containing two cysteines, then binds to the catalytic

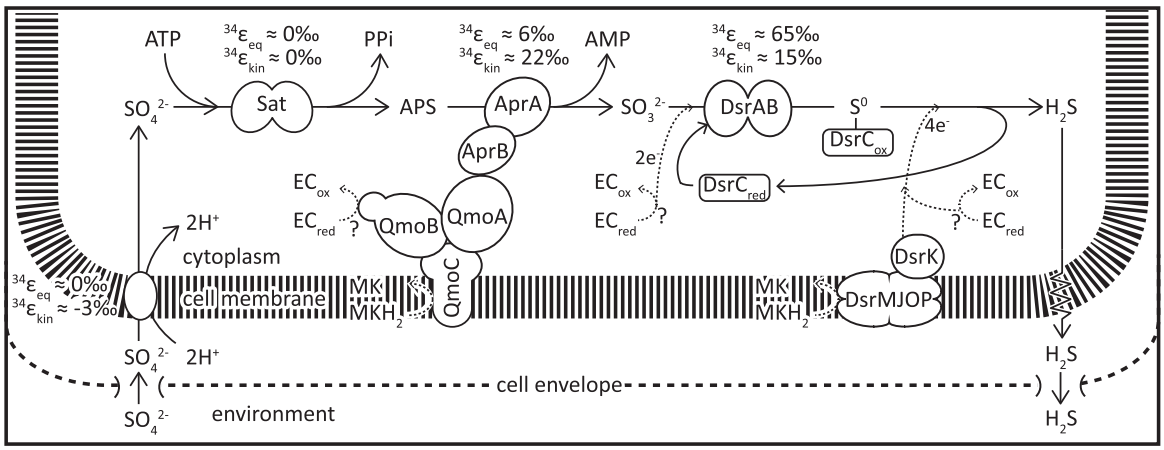

Figure 1 Simplified illustration of the dissimilatory sulfate reduction network and S isotope fractionation associated with each reaction step. Proposed modes of electron flow are indicated with dashed arrows. See text for a detailed description. $^{34}\varepsilon_{eq}$, equilibrium S isotope fractionation; $^{34}\varepsilon_{kin}$, kinetic S isotope fractionation; Apr, APS reductase; Dsr, dissimilatory sulfite reductase; EC_{red}, reduced electron carrier; EC_{ox}, oxidized electron carrier; MK, menaquinone; MKH_2, menaquinol; Sat, sulfate adenylyl transferase. The figure is adapted from Wing and Halevy (2014) and includes new insights into the DsrC cycle from Santos *et al.* (2015).

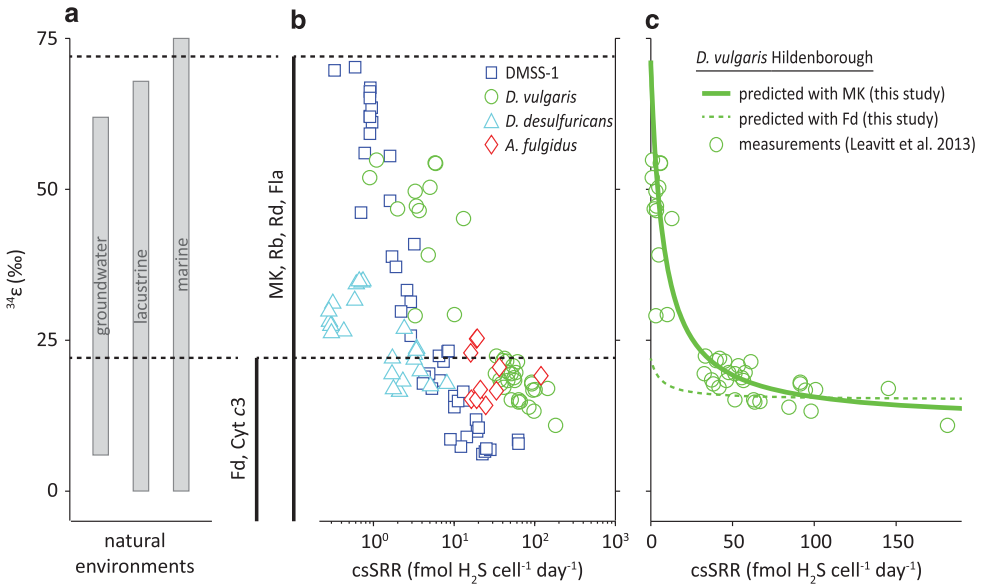

Figure 2 Predicted (this study) and experimentally determined (previously reported) rate-fractionation relationships during DSR. (**a**) Reported range of S isotope fractionation from natural environments (data compiled in Sim *et al*., 2011a) and (**b**) rate-fractionation relationships determined in pure culture experiments with DMSS-1 (Sim *et al*., 2011a, b, 2012), *D. vulgaris* Hildenborough (Leavitt *et al*., 2013), *D. desulfuricans* (Chambers *et al*., 1975) and *A. fulgidus* (Habicht *et al*., 2005) grown on organic substrates. The magnitude of S isotope fractionation increases with decreasing csSRR. The black vertical lines indicate the possible range of S isotope fraction allowed by the respective electron carriers (determined in this study). The full range of environmental and experimental fractionation is reproducible with electron carriers with modestly negative reduction potentials such as for example, menaquinone (MK). Ferredoxin (Fd) as a direct electron donor would limit the maximum fractionation to <22‰, which is inconsistent with reported experimental data at low csSRR. (**c**) Predicted rate-fractionation relationship with menaquinone (solid line) and ferredoxin (dashed line) as electron carrier vs. experimental data (markers) from experiments with *D. vulgaris* Hildenborough (Leavitt *et al*., 2013). Cyt *c*3, cytochrome *c*3; Fla, flavodoxin; Rb, rubredoxin; Rd, rubrerythrin.

site, transfers two additional electrons to the S^{II} intermediate and eventually forms a DsrC-bound S^0 trisulfide product, in which the S^0 originates from SO_3^{2-} and forms a bridge between the two cysteines (Santos *et al*., 2015). In a next step, this DsrC-bound S^0 trisulfide is reduced to H_2S and DsrC. The reaction requires a total of 4 electrons, 2 for the reduction of S^0 to H_2S, and 2 to recycle DsrC. Although this reaction is partly catalyzed by a membrane-bound DsrMKJOP complex, implicating the oxidation of menaquinol, other electron carriers have been proposed (Oliveira *et al*., 2008; Venceslau *et al*., 2014; Santos *et al*., 2015).

In addition to ferredoxin and menaquinone, a number of other electron carriers—rubredoxin, flavodoxin, cytochrome *c*3 and rubrerythrin—have been identified in many SROs (Odom and Peck, 1984; Fauque *et al*., 1988; Kremer *et al*., 1988; Rabus *et al*., 2006; Ramos *et al*., 2012; Price *et al*., 2014b; Rabus *et al*., 2015; Dörries *et al*., 2016). Likewise, several transmembrane redox complexes, such as Hmc, Tmc, Ohc or Rnf are found in many SROs, although their function is only partly understood (Pereira *et al*., 2011). Most insights into the physiology of sulfate reducing organisms, as well as predictions and speculations about the physiological role of electron carriers, have been based on pure cultures grown under optimal conditions (high-energy availability, fast growth). How these findings relate to organisms living in natural low-energy environments is unclear. Investigation of the variability in isotope fractionation in natural low-energy environments as well as in pure cultures has the potential to shed new light on this fundamental question.

Large S isotope fractionation is common in natural energy-limited environments

Sulfate-reducing microbes preferentially process S-bearing metabolites containing the light stable isotope of S, ^{32}S, leaving the residual sulfate enriched, and the product sulfide depleted, in ^{34}S. The degree of this fractionation during DSR is quantified as $^{34}\varepsilon = (^{34}\alpha - 1) \times 1000$ (in permil, ‰), where $^{34}\alpha = (^{34}S/^{32}S)_{sulfate}/(^{34}S/^{32}S)_{sulfide}$. In laboratory cultures, $^{34}\varepsilon$ ranges from -3‰ to 72‰ (Kaplan and Rittenberg, 1964; Chambers *et al*., 1975; Habicht and Canfield, 2001; Wortmann *et al*., 2001; Sim *et al*., 2011b, 2012; Leavitt *et al*., 2013). The upper end of this range is proposed to reflect near-thermodynamic equilibrium fractionation (Wing and Halevy, 2014) and is accessed in the laboratory only at the lowest growth rates and cell-specific sulfate reduction rates (csSRR) (Sim *et al*., 2012).

Large, near-thermodynamic S isotope fractionations associated with DSR are also observed in low-energy niches in many natural environments (Figure 2), including intertidal mudflats (Böttcher *et al*., 2000), lakes (Ivanov *et al*., 2001), coastal

environments (Kaplan *et al.*, 1963; Goldhaber and Kaplan, 1975), continental shelves (Wortmann *et al.*, 2001), deep sea sediments (Böttcher *et al.*, 2004; Orsi *et al.*, 2016) and euxinic water columns (Werne *et al.*, 2003). In the majority of these environments, the quality of the low-molecular weight organic compounds that support DSR is poor and, as a result, csSRR is low and the observed S isotope fractionations are large. Understanding the energetics that allows ubiquitously large fractionations thus has the potential to shed light on the physiology and metabolism of the majority of sulfate reducers in natural environments.

Materials and methods

Below we outline our theoretical approach. A detailed description of the model, underlying experimental datasets, and sensitivity analyses can be found in the Supplementary Information and in Wing and Halevy (2014). All acronyms used are summarized in Table 1.

Electron carrier identity impacts the maximal whole-organism S isotope fractionation

The magnitude of whole-organism S isotope fractionation during DSR varies with temperature, the carbon source, and sulfate availability (Bruchert *et al.*, 2001; Canfield, 2001; Habicht and Canfield, 2001; Johnston *et al.*, 2007; Sim *et al.*, 2011b; Bradley *et al.*, 2016). In addition, many studies have shown that the magnitude of S isotope fractionation correlates inversely with csSRR (Figure 2) (Harrison and Thode, 1958; Kaplan and Rittenberg, 1964; Chambers *et al.*, 1975; Sim *et al.*, 2011a, b, 2012; Leavitt *et al.*, 2013). This range of S isotope fractionation magnitude has been related to the reversibility of the individual steps in the sulfate reduction pathway (Rees, 1973; Brunner and Bernasconi, 2005; Bradley *et al.*, 2011; Wing and Halevy, 2014).

Table 1 Nomenclature

Acronym	*Description*
DSR	Dissimilatory sulfate reduction
SRO	Sulfate-reducing organism
EC	Electron carrier
$R_{r/o}$	Ratio of reduced to oxidized electron carrier concentrations
csSRR	Cell-specific sulfate reduction rate
$\Delta G'^{\circ}$	Standard Gibbs free energy
E'°	Standard reduction potential
K_M	Michaelis–Menten half saturation concentrations
α^{eq}	Equilibrium fractionation factor
α^{kin}	Kinetic fractionation factor
$^{34}\varepsilon$	S isotope enrichment factor;$^{34}\ \varepsilon = (\alpha - 1) \times 1000$
MK	Menaquinone
Rb	Rubredoxin
Rd	Rubrerythrin
Fla	Flavodoxin
Cyt *c*3	Cytochrome *c*3
Fd	Ferredoxin

Briefly, in DSR, SO_4^{2-} is transported into the cytoplasm, activated with ATP to form APS, which is then reduced to SO_3^{2-} and ultimately to H_2S:

$$\underset{SO_4^{2-}\,(out)}{A} \underset{\phi_{BA}}{\overset{\phi_{AB}}{\rightleftarrows}} \underset{SO_4^{2-}\,(in)}{B} \underset{\phi_{CB}}{\overset{\phi_{BC}}{\rightleftarrows}} \underset{APS}{C} \underset{\phi_{DC}}{\overset{\phi_{CD}}{\rightleftarrows}} \underset{SO_3^{2-}}{D} \underset{\phi_{ED}}{\overset{\phi_{DE}}{\rightleftarrows}} \underset{H_2S,}{E} \quad (1)$$

where ϕ_{AB}, for example, is the flux from A (extracellular SO_4^{2-}) to B (intracellular SO_4^{2-}). The overall isotope fractionation, $^{34}\alpha_{A,E}$, can be expressed as:

$$^{34}\alpha_{A,E} = f_{BA} \times \left(^{34}\alpha^{eq}_{A,B} \times {}^{34}\alpha_{B,E} - {}^{34}\alpha^{kin}_{A,B} \right) + {}^{34}\alpha^{kin}_{A,B}, \quad (2)$$

$$^{34}\alpha_{B,E} = f_{CB} \times \left(^{34}\alpha^{eq}_{B,C} \times {}^{34}\alpha_{C,E} - {}^{34}\alpha^{kin}_{B,C} \right) + {}^{34}\alpha^{kin}_{B,C}, \quad (3)$$

$$^{34}\alpha_{C,E} = f_{DC} \times \left(^{34}\alpha^{eq}_{C,D} \times {}^{34}\alpha_{D,E} - {}^{34}\alpha^{kin}_{C,D} \right) + {}^{34}\alpha^{kin}_{C,D} \quad (4)$$

$$^{34}\alpha_{D,E} = f_{ED} \times \left(^{34}\alpha^{eq}_{D,E} - {}^{34}\alpha^{kin}_{D,E} \right) + {}^{34}\alpha^{kin}_{D,E} \quad (5)$$

where α^{eq} are the equilibrium isotope fractionations ($\alpha^{eq} \equiv R_{reactant}/R_{product}$, where R is $^{34}S/^{32}S$, in a reactant or product in isotopic equilibrium) and α^{kin} are the kinetic isotope fractionations ($\alpha^{kin} \equiv {}^{32}k/{}^{34}k$, where ^{32}k and ^{34}k refer to the enzymatic reaction rate constants of the light and heavy isotopologues) of each step. The net fractionation of each step varies between α^{eq} and α^{kin} depending on the value of f, the reversibility, which is defined as the ratio of the reverse to forward flux in the reaction (for example, ϕ_{BA}/ϕ_{AB} in the leftmost reaction in reaction network 1) and varies from unity at equilibrium to zero for a completely unidirectional reaction.

For each step during DSR, α^{eq} can be calculated theoretically (Bigeleisen and Mayer, 1947; Urey, 1947; Otake *et al.*, 2008; Eldridge *et al.*, 2016) for a given temperature (here 25 °C if not stated differently, the experimental temperature of the rate-fractionation study with the model sulfate reducer *Desulfovibrio vulgaris* (Leavitt *et al.*, 2013)). Constraints on α^{kin} are poorer. Sulfate uptake into the cell and its subsequent activation to APS seem to have a $^{34}\alpha^{kin}$ close to unity (Harrison and Thode, 1958) (Figure 1). The following reduction steps, however, discriminate against ^{34}S leading to a measurable fractionation in the intermediate substrates (Harrison and Thode, 1958; Kemp and Thode, 1968; Leavitt *et al.*, 2015). This ^{34}S depletion in the cell's internal metabolite pools will only be expressed as a relative ^{34}S enrichment in the residual extracellular sulfate pool if all preceding steps are to some degree reversible (that is, if f in equations 2,3,4,5 is not close to zero; see Supplementary Information for a detailed discussion on the reversibility of enzymatic reactions).

The reversibility, f, is linked to the actual free energy of a reaction (ΔG_r) via the flux–force theorem

(Beard and Qian, 2007):

$$f_{\mathrm{pr}} = \frac{\Phi_{\mathrm{reverse}}}{\Phi_{\mathrm{forward}}} = e^{\frac{\Delta G_{\mathrm{r}}}{RT}}, \quad (6)$$

where R is the gas constant and T the temperature. Importantly, ΔG_{r} depends on the standard-state Gibbs free energy ($\Delta G'^{\circ}$) and on the concentrations of intracellular metabolites:

$$\Delta G_{\mathrm{r}} = \Delta G'^{\circ} + RTln\left(\frac{\prod_i [p_i]^{m_i}}{\prod_j [r_j]^{n_j}}\right), \quad (7)$$

where $[p_i]$ and $[r_j]$ are the concentrations, and m_i and n_j the stoichiometric coefficients, of the product i and reactant j, respectively. In combination with enzyme kinetic principles (Flamholz *et al*., 2013), this shows that net S isotope fractionations are under the proximate control of the energetics and kinetics of the S reactions, as they govern the relative levels of the S-bearing metabolites for a given csSRR.

The prescribed csSRR can be thought of as encompassing the effects of substrate availability and quality, and the partitioning of energy yield between cellular function and growth, albeit without an explicit account for the dependence of csSRR on these factors. We used the link between the expressed net fractionation at low csSRR and ΔG_r of the reactions in the DSR network to constrain the identity of the electron carriers used during APS and SO_3^{2-} reduction in their natural low-energy environment. As the standard reduction potential (E'°) of the electron carriers is a major component of ΔG_{r}, reproduction of the large isotopic fractionations at low csSRR place direct limits on the reduction potential of the electron carriers involved and, therefore, on their identity.

Results and discussion

We find that large S isotope fractionations, such as those observed in natural environments (Figure 2a) and in pure culture experiments at low respiration rates (Figure 2b), are only possible with electron carriers with modestly negative reduction potentials. Moreover, menaquinone, rubredoxin, rubrerythrin and some flavodoxins not only allow large S isotope fractionation at low csSRR, but also predict specific csSRR-fractionation relationships that have been observed in pure culture experiments (Figure 2c). Electron carriers with strongly negative reduction potentials (for example, ferredoxin) limit the maximum achievable fractionation to less than 22‰, which is inconsistent with laboratory and natural data at low csSRR (Figure 2).

Three parameters exert primary control on the magnitude of S isotope fractionation at a given csSRR: electron carrier identity ($\Delta G'^{\circ}$), $R_{r/o}$ and K_M values

We identified two criteria that must be fulfilled by any proposed energy metabolism scheme for DSR (Supplementary Table S1). First, large S isotope fractionation (>55‰) must be achieved at prescribed low respiration rates (~0.1 fmol H_2S per cell per day). Second, intracellular metabolite concentrations, namely $[SO_4^{2-}]_{\mathrm{in}}$, [PPi], [APS] and $[SO_3^{2-}]$, must be within physiological limits (10^{-9} to 10^{-3} M).

Although the second criterion sets the physiological limits of our model, the first criterion constrains the energetics that allows DSR to operate in a net forward direction, but close enough to thermodynamic equilibrium that large isotopic fractionations are possible, as observed in natural environments. Large isotope fractionations are only possible when the reversibility terms, f, in equations 2,3,4,5 approach unity (Figure 1). To identify the parameters controlling reversibility, we combined equations 6 and 7 with expressions for the net rate of each reaction and solved for f (see Supplementary Information for a complete derivation). By doing so, three parameters emerged as possible controls on the reversibility of each reaction at a specific respiration rate: (i) the standard-state Gibbs free energies, $\Delta G'^{\circ}$, for each of the reactions, (ii) the ratio of reduced to oxidized electron carrier concentrations ($R_{r/o} = [EC_{red}]/[EC_{ox}]$, where EC stands for electron carrier) for APS and SO_3^{2-} reduction, and (iii) the Michaelis–Menten half-saturation concentrations (K_M) of the sulfur-bearing metabolic substrates.

The first of these controls ($\Delta G'^{\circ}$) can be calculated directly from the reduction potential of the half-reactions for the respective electron carriers at standard-state conditions. After calculating $\Delta G'^{\circ}$ for a wide range of electron carriers suggested to participate in APS and SO_3^{2-} reduction schemes, we varied the second and third controls, $R_{r/o}$ and K_M, to extremal values and explored the dependence of the maximum achievable S isotope fractionation on these parameters. This exercise showed that the influence of $R_{r/o}$ and K_M is co-dependent and critically affected by the values calculated for $\Delta G'^{\circ}$. Thus, we start with a discussion of the identity of the electron carriers and energy supply schemes that enable large fractionation at low csSRR. We then explore the interplay among $R_{r/o}$, K_M values, and electron carrier identity and use the second criterion —reasonable intracellular metabolite concentrations —to place physiological limits on $R_{r/o}$.

Large S isotope fractionation requires electron carriers with small-magnitude reduction potentials

The observation of large fractionation (>55‰) at low respiration rates (~0.1 fmol H_2S per cell per day) requires nearly full reversibility of all steps during DSR (Figure 1; Equations 2,3,4,5). Assuming default values for $R_{r/o}$ and K_M (Supplementary Tables S4 and S5), full reversibility of APS and SO_3^{2-} reduction is only possible when electron carriers with modestly negative reduction potentials are involved in DSR (Figures 3a and 4a). Specifically, the standard-state Gibbs free energy ($\Delta G'^{\circ}$) of APS and SO_3^{2-} reduction

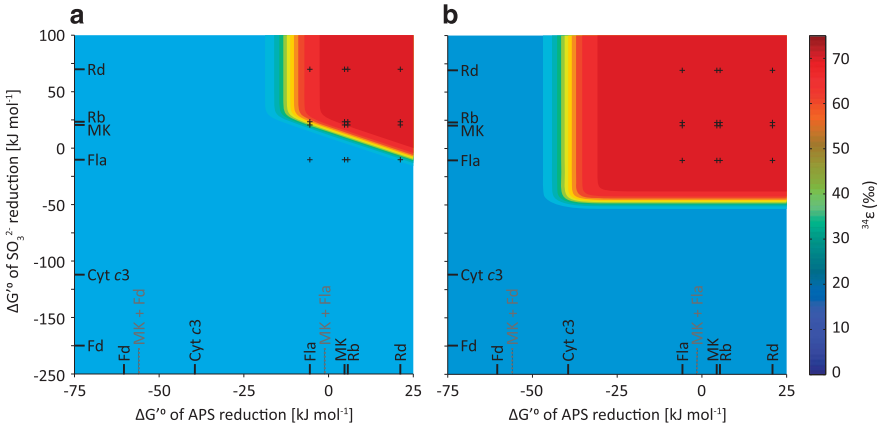

Figure 3 Maximum achievable S isotope fractionation at low csSRR for (**a**) reasonable, and (**b**) extreme conditions (see Supplementary Table S5, Supplementary Figure S1 and Supplementary Dataset S1). Even with extreme values for $R_{r/o}$ and K_M large fractionation is only possible when $\Delta G'^{\circ}$ of APS reduction > -40 kJ mol^{-1} and $\Delta G'^{\circ}$ of SO_3^{2-} reduction > -50 kJ mol^{-1}. The black ticks and text indicate the calculated $\Delta G'^{\circ}$ of the reaction with the respective electron carrier; the dashed grey lines and text indicate the calculated $\Delta G'^{\circ}$ of the reaction with the respective electron carriers in potential electron confurcation schemes. A confurcation scheme of ferredoxin and menaquinone for APS reduction, for example, limits the possible range of isotope fractionation to less than 22‰ and is therefore inconsistent with observations. csSRR = 0.1 fmol H_2S per cell per day; $R_{r/o}$ = 20 (**a**) or 0.001 (**b**). Reasonable and extreme K_M values are listed in Supplementary Table S5. Standard redox potentials for the electron carriers are given in Supplementary Table S3. Cyt *c*3, cytochrome *c*3; Fd, ferredoxin; Fla, flavodoxin (with a modestly negative reduction potential); MK, menaquinone; Rb, rubredoxin; Rd, rubrerythrin.

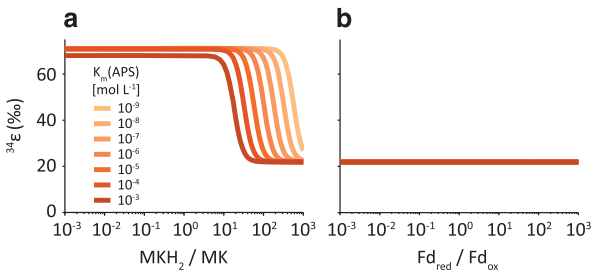

Figure 4 Maximum achievable S isotope fractionation as a function of reduced to oxidized electron carrier concentration ratios at low csSRR (0.1 fmol H_2S per cell per day). The electron carrier involved in both APS and SO_3^{2-} reduction is (**a**) menaquinone and (**b**) ferredoxin. For menaquinone, fractionation at low $R_{r/o}$ plateaus at ~72‰, the sulfate-sulfide equilibrium fractionation. For ferredoxin, APS (and SO_3^{2-} reduction) remain irreversible even at low $R_{r/o}$ and the maximum fractionation reaches ~22‰, the sum of the sulfate-APS equilibrium fractionation and the kinetic fractionation of APS reduction.

must each be less negative than approximately -10 kJ mol^{-1}. When electron carriers with strongly negative reduction potentials are involved, the $\Delta G'^{\circ}$ of these reactions is more negative, and they operate far from equilibrium, leading to net S isotope fractionations that are much smaller than the thermodynamic limit. In principle, at a low enough csSRR, DSR should operate close to thermodynamic equilibrium and isotope fractionations should be large, irrespective of the electron carrier involved. However, the limitation of the maximal fractionation described above occurs even at csSRR as low as 10^{-4} fmol H_2S per cell per day, equivalent to the lowest rates observed in natural environments (Hoehler and Jørgensen, 2013).

Variation of $R_{r/o}$ and K_M values may expand the range of possible electron carriers, but even when these parameters are varied to extremes (see Supplementary Information) the involvement of some electron carriers limits the possible range of fractionation to less than 22‰. Specifically, variation of $R_{r/o}$ and K_M values permits a standard-state Gibbs free energy ($\Delta G'^{\circ}$) of APS reduction greater than -40 kJ mol^{-1} and that of SO_3^{2-} reduction > -50 kJ mol^{-1} (Figure 3b). Any potential electron transfer scheme must meet this requirement. Below we discuss first the constraints that this places on the involvement of any single physiological electron carrier, and then the implications for the existence of proposed electron supply schemes.

Most SROs have genes encoding for a wide range of electron carriers. Similarly, environmental metagenome analyses, as well as transcriptome studies from a variety of environments reveal a large range of metabolic potential of the respective communities (Keller and Wall, 2011; Zhou *et al.*, 2011; Orsi *et al.*, 2013; Lau *et al.*, 2016; Orsi *et al.*, 2016). The requirement for small-magnitude reduction potential described here means that some proposed electron carriers, such as ferredoxin, cannot be the direct electron donors for APS and SO_3^{2-} reduction, at least at low csSRR. Instead, menaquinone, rubredoxin, or rubrerythrin might be involved in DSR, because of their slightly negative to positive reduction potential. Membrane-associated menaquinones have been found in most SROs (Collins and Widdel, 1986; Tindall *et al.*, 1989) and are essential for the reduction of APS at least in *Desulfovibrio alaskensis* (Keller *et al.*, 2014). Menaquinol (MKH_2) oxidation during DSR is thought to be coupled to H^+ release into the periplasm, contributing to the establishment of a proton gradient across the cytoplasmic membrane that can further be used for ATP generation

(Pires *et al.*, 2003; Venceslau *et al.*, 2010; Keller *et al.*, 2014). Although this proposed physiological function and the widespread occurrence of menaquinones across SROs suggests their involvement in DSR, their feeble reduction potential often results in their rejection as sole electron carriers in favor of more robust electron sources. Our results, however, show that isotope fractionation can reconcile the omnipresence and small reduction potential of menaquinones during DSR.

Rubredoxins are also present in most sulfate-reducing prokaryotes and are also possible components of the electron transport chain supplying DSR (Odom and Peck, 1984). They are small proteins, containing an iron center and four cysteine residues and have been purified from the cytoplasmic fractions of all known *Desulfovibrio* strains (Bell *et al.*, 1974; Odom and Peck, 1984; LeGall and Peck, 1987; Moura *et al.*, 1999). The identification of a NADH: rubredoxin oxidoreductase in *Desulfovibrio gigas* is a compelling argument for a role of rubredoxin in energy conservation in sulfate-reducing prokaryotes (LeGall, 1968; Odom *et al.*, 1976; Kremer *et al.*, 1988). Likewise, rubrerythrin has been purified from several sulfate-reducing bacteria (LeGall *et al.*, 1988; deMaré *et al.*, 1996; Moura *et al.*, 1999) and its encoding genes are highly expressed during growth of *Archaeoglobus fulgidus* (Hocking *et al.*, 2014). Its function during DSR is poorly understood, and rubrerythrin as well as rubredoxin are perhaps involved in oxidative stress mitigation rather than in electron transport to the S intermediates (Lumppio *et al.*, 2001). The suggested physiological function of rubrerythrin and rubredoxin as part of an oxidative stress mitigation system, however, should be reconsidered given the high abundance of their gene transcripts expressed by SROs in anaerobic deep-subsurface environments (Lau *et al.*, 2016; Orsi *et al.*, 2016). In fact, in the same metatranscriptome datasets, genes that encode typical oxidative stress mitigation systems, such as superoxide reductase or glutathione peroxidase, were not upregulated (Lau *et al.*, 2016; Orsi *et al.*, 2016). This suggests that oxygen contamination during sampling did not significantly affect the results, and that a role for rubrerythrin and rubredoxin in SROs other than oxidative stress mitigation should be considered.

It is important to note that from a purely isotopic perspective, any electron carrier with a standard reduction potential greater than approximately -220 mV will result in modestly negative $\Delta G'^{\circ}$ of the redox reactions and could therefore serve as the physiological electron donor to APS and SO_3^{2-} reductase at low csSRR (Figure 3, Supplementary Table S3). Flavodoxins, for example, have two oxidation states with reduction potentials of E'° F/FH ≈ -115 mV and E'° FH/FH_2 ≈ -371 mV, respectively (Thauer *et al.*, 1977). It is hence possible that at low csSRR FH oxidation, but not FH_2 oxidation, drives the reduction of APS or SO_3^{2-}. Similarly, several types of ferredoxins are known, for example, ferredoxin I and ferredoxin II in *D. gigas*, with reduction potentials of -398 mV and -130 mV, respectively (Odom and Peck, 1984). Ferredoxin II with a modestly negative reduction potential is expressed by some, but not all, SROs (Pereira *et al.*, 2011). By contrast, ferredoxin I with a strongly negative reduction potential seems to be a conserved protein among all SROs (Pereira *et al.*, 2011) and is hence ascribed an important role in the overall electron transport chain during DSR (Ramos *et al.*, 2012; Grein *et al.*, 2013; Hocking *et al.*, 2014; Keller *et al.*, 2014; Price *et al.*, 2014b; Rabus *et al.*, 2015). Moreover, several ferredoxin-reducing enzymes have been identified in sulfate reducers such as ferredoxin:NADH or pyruvate:ferredoxin oxidoreductases (Ogata and Yagi, 1986; Keller and Wall, 2011; Pereira *et al.*, 2011; Rabus *et al.*, 2013) and in experiments with *D. alaskensis* G20 the generation of reduced ferredoxin proved to be important for fitness (Price *et al.*, 2014b). However, although ferredoxin I is ubiquitously present among sulfate reducers, its physiological function remains unclear. The strongly negative reduction potential of ferredoxin I means it cannot be the direct electron donor to APS and SO_3^{2-} reductase (with the exception of a specific electron transfer scheme to DsrAB as outlined below), at least at low respiration rates. Instead, it is possible that at least in some SROs, ferredoxin II could replace ferredoxin I in its function and drive APS or SO_3^{2-} reduction. In general, ferredoxins (I or II) may also be indirectly involved in DSR by acting as electron capacitors and regulating the redox poise of the direct electron donor to sulfate reduction intermediates. Such a potential indirect involvement of ferredoxin is not explicitly treated in our model and can thus not be excluded.

In summary, our findings are in line with recent observations from anoxic deep-subsurface environments, where relatively high abundance of electron carrier-encoding gene transcripts, which in laboratory experiments are associated with oxidative stress mitigation, have been found. Our predictions, although in agreement with observational data from low-energy environments, directly challenge energetic arguments that are often used to evaluate the role of various electron carriers involved in APS and SO_3^{2-} reduction. In general, it is assumed that if one intracellular redox reaction during DSR is more exergonic at standard state than another, then it is more likely to occur in living cells. However, cells do not live at standard state, and can have intracellular metabolite concentrations that are many orders-of-magnitude different than standard values. As long as a net metabolic reaction is energetically favorable, intracellular metabolite concentrations adjust within physiological limits to allow net forward fluxes (albeit close to thermodynamic equilibrium) for all intermediate reactions, even for those that are unfavorable at standard-state conditions (Milo and Phillips, 2015).

Moreover, from a thermodynamic perspective, bacterial growth is most efficient when the energetic requirements for biomass synthesis and maintenance of cellular functions are balanced by energy production from the respiring processes (von Stockar *et al.*, 2006). In other words, at a small ΔG of the overall metabolic reactions, which is generally the case in the subsurface biosphere, higher respiration rates are possible when using electron carriers with modestly negative reduction potential (Supplementary Figure S2). This is because less of the available ΔG is dissipated in inefficient redox reactions. We suggest that as ATP production is proportional to the total respiration (here sulfate reduction) rate, electron carriers with modestly negative reduction potential allow production of enough ATP for survival at a smaller environmental ΔG (that is, under less favorable conditions) than do strongly negative reduction potential electron carriers (Supplementary Figure S2).

Large S isotope fractionation constrains possible electron supply schemes

The paradigm that more energetic standard-state reactions are more biologically relevant has led to the conclusion that, for example, rubredoxins are unlikely electron carriers during DSR because of their rather positive reduction potentials (Rabus *et al.*, 2006). Similarly, it has been argued that menaquinone ($E'^\circ = -74$ mV) cannot be the single electron donor to APS reduction, because of the apparently unfavorable energetics of the reaction at standard-state conditions (Ramos *et al.*, 2012; Grein *et al.*, 2013; Keller *et al.*, 2014; Rabus *et al.*, 2015). As a result, a second electron donor with a strongly negative reduction potential is invoked to drive the APS reduction reaction in a so-called electron confurcation scheme (Ramos *et al.*, 2012; Grein *et al.*, 2013; Keller *et al.*, 2014). The most commonly assumed confurcation partner donating electrons to APS is ferredoxin ($E'^\circ = -398$ mV), even though its direct involvement has yet to be demonstrated. We find that at least at low csSRR and in organisms that display large S isotope fractionations, ferredoxin with its strongly negative reduction potential cannot be the confurcation partner. A confurcation scheme of menaquinol and ferredoxin, each donating one electron to the reduction of APS, results in a $\Delta G'^\circ$ of -56 kJ mol^{-1} for this reaction (Figure 3). This leads to a kinetic control of APS reduction even at very low respiration rates and limits the achievable range of isotope fractionation to less than 22‰, which is inconsistent with observations. Our results support the inference that menaquinol oxidation can reduce APS through the QmoABC and AprAB complexes without the involvement of a third partner (Duarte *et al.*, 2016). Our approach places firm limits on the electron confurcation schemes that are possible for APS reduction; a viable scheme must have $\Delta G'^\circ > -40$ kJ mol^{-1} (for example, menaquinol + flavodoxin; Figure 3b), at least at low csSRR.

The electron budget during SO_3^{2-} reduction has recently been clarified (Santos *et al.*, 2015). The first two electrons for SO_3^{2-} reduction are likely transferred from an unknown electron carrier, whereas the latter four ultimately originate from menaquinol oxidation (Figure 1; Santos *et al.*, 2015). From the calculated $\Delta G'^\circ$ of this specific scenario (Supplementary Table S2, Supplementary Table S3) and the requirement that $\Delta G'^\circ > -10$ kJ mol^{-1}, we conclude that only a few electron carriers, the ones with $E'^\circ > -220$ mV, are potential candidates for transferring the first two electrons to DsrAB (menaquinone, rubredoxin, rubrerythrin and some flavodoxins; Figure 3a and Supplementary Table S3). Similarly, any proposed electron bi- or confurcation scheme involved in DsrC recycling must meet the requirement of $\Delta G'^\circ > -10$ kJ mol^{-1} for the net reaction, or else it will result in small S isotope fractionations at low csSRR. With default $R_{r/o}$ and K_M values, we find that no such scheme allows large fractionation at low csSRR. Allowing extreme ranges of K_M values and $R_{r/o}$ significantly expands the list of possible electron carriers transferring the first two electrons to DsrAB. In this case, it appears that the requirement of $\Delta G'^\circ > -50$ kJ mol^{-1} is met with all of the investigated electron carriers (Supplementary Table S3). For example, with ferredoxin transferring the first 2 electrons to the reduction of SO_3^{2-} and the remaining four ultimately originating from menaquinol oxidation, we calculate a $\Delta G'^\circ$ of -41 kJ mol^{-1} for the overall redox reaction. Although this value allows large fractionation at low csSRR, it requires $R_{r/o}$ to be <0.05 and an extremely low affinity ($K_M(H_2S) \geqslant 100$ mM) of Dsr toward H_2S (Figure 3b and Supplementary Table S5). Importantly, if future experimental results show that $R_{r/o}$ and $K_M(H_2S)$ indeed take such values, our results suggest a direct physiological role for ferredoxin in SO_3^{2-} reduction, instead of, or in addition to, its proposed regulatory function as electron capacitor.

S isotope fractionation and physical limits constrain intracellular $R_{r/o}$ values to a narrow range

We have shown that large S isotope fractionation at low csSRR is possible only if electron carriers with slightly negative to positive reduction potentials are involved in DSR, even when all other parameters in the bio-isotopic model were allowed to vary to extremes. Importantly, K_M values are relatively well constrained from independent biochemical analyses in several sulfate reducing bacteria and archaea (Supplementary Table S5 and Supplementary Dataset S1) and we adopted literature K_M values for most cases. In contrast to the relatively well-constrained K_M values, information on the ratio of reduced to oxidized electron carriers, $R_{r/o}$, is rare, and so we explored the influence of this parameter in more detail.

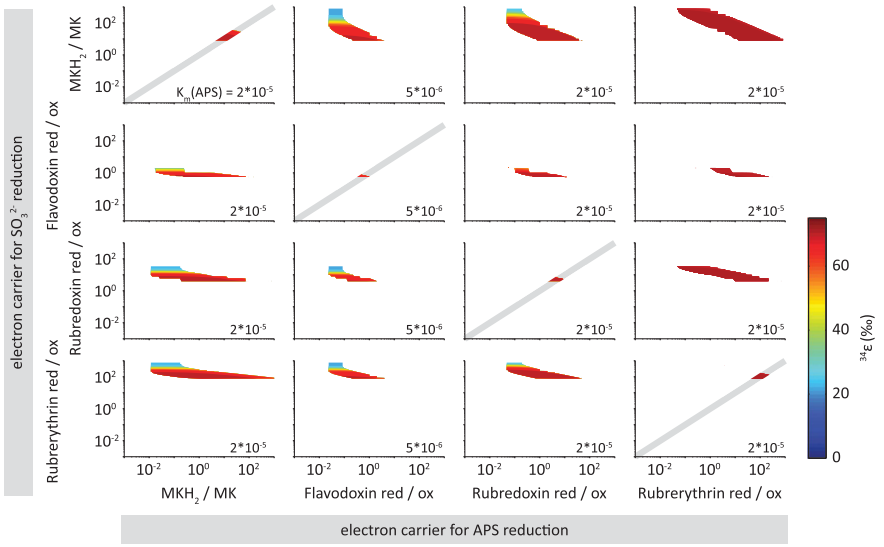

Figure 5 The range of $R_{r/o}$ yielding reasonable (1 nM–1 mM) intracellular metabolite concentrations. Results are shown only for electron carriers that allow near-thermodynamic fractionations at low csSRR. Columns and rows show electron carriers for APS and SO_3^{2-} reduction, respectively. White space indicates combinations of $R_{r/o}$ that produce unreasonable intracellular metabolite concentrations over some or all of the range of csSRR accessed in culture experiments (0.1 to 125 fmol H_2S per cell per day). Colored contours indicate the magnitude of net isotope fractionation at a csSRR of 0.1 fmol H_2S per cell per day and with values of K_M for APS at Apr shown in the lower right corner of each panel. Other K_M were at their default values (Supplementary Table S5). When the same electron carrier is involved in both APS and SO_3^{2-} reduction (on the diagonal), the possible range of $R_{r/o}$ is further constrained to be on the solid grey line.

Only a relatively narrow range of $R_{r/o}$ values affects the reversibility of the electron transfer reactions, and therefore the net S isotope fractionation (Figure 4). For a given electron carrier, S isotope fractionation transitions from a plateau to a floor across a narrow, approximately tenfold change in $R_{r/o}$ values. The threshold values of $R_{r/o}$ at which the fractionation transition occurs is weakly dependent on the K_M values for the enzymatic redox reactions in DSR (Figure 4). In the case of menaquinone as sole electron carrier in DSR, for example, maximum S isotope fractionation approaches 72‰ at low csSRR (~0.1 fmol H_2S per cell per day; Figure 4a). Above a certain threshold of $R_{r/o}$, however, the energetics of APS reduction become increasingly favorable and this reaction departs from equilibrium, resulting in a kinetically controlled net S isotope fractionation of only 22‰ (Figures 1 and 4a, and Equations 2,3,4). The same kinetic control of APS reduction is observed when ferredoxin is the sole electron carrier, resulting again in net S isotope fractionation of 22‰ (Figure 4b). In this case, however, the maximum fractionation remains at 22‰, independent of the value of $R_{r/o}$.

Importantly, in both of the above examples, the identity of the physiological electron carriers involved governs the S isotope fractionation achieved on the floor and plateau, but the $R_{r/o}$ and K_M values determine the precise location of the transition in the fractionation landscape. Thus, the theoretical exercise of choosing extremely low values for $R_{r/o}$ places the allowable fractionation on the plateau, and increases the range of electron carriers that allow large fractionation at low csSRR. However, extreme values of $R_{r/o}$ may violate our second criterion—reasonable intracellular metabolite concentrations. A combination of large fractionation at low csSRR and plausible intracellular metabolite concentrations can, therefore, constrain the physiological values of $R_{r/o}$.

To restrict possible ranges of $R_{r/o}$, we require that all intracellular metabolite concentrations never drop below 1 nM, which for typical sulfate reducer volumes would mean less than a single molecule in the cell, and never exceed 1 mM. We further allow different electron carriers to be involved in APS and SO_3^{2-} reduction, resulting in different $R_{r/o}$ values for these two reactions. For a given combination of electron carriers we vary each $R_{r/o}$ from 10^{-3} to 10^{3} and calculate the net S isotope fractionation ($^{34}\varepsilon$) and intracellular metabolite concentrations, (that is, $[SO_4^{2-}]_{in}$, [APS], [PPi] and $[SO_3^{2-}]$). Figure 5 shows the calculated $^{34}\varepsilon$ at a csSRR of 0.1 fmol H_2S per cell per day for cases in which all metabolite concentrations fall in the range between 1 nM and 1 mM at csSRR between 0.1 and 125 fmol H_2S per cell per day. The white space indicates parameter combinations that lead to metabolite concentrations outside these boundaries. In all cases, we are left with a relatively narrow range of possible values for $R_{r/o}$. When the same electron carriers are involved in APS and SO_3^{2-} reduction, the possible values for $R_{r/o}$ are even more tightly constrained (indicated by the grey 1:1 lines in Figure 5). For example, if menaquinone is the electron carrier involved in both APS and SO_3^{2-} reduction, then $R_{r/o}$ (MKH$_2$/MK) must lie in the range between ~10 and ~30 for large isotope fractionation at low csSRR, with plausible metabolite concentrations (Figure 5 upper left panel).

In summary, we have identified a set of low-potential electron carriers, $R_{r/o}$, and K_M values that permit large S isotope fractionation at low csSRR, and at reasonable intracellular metabolite concentrations. Importantly, this set of parameters allows not only large fractionation at low csSRR, but also reproduction of the full set of $^{34}\varepsilon$ values (−3‰ to 72‰) observed over the range of csSRR seen in nature and in culture (Figure 2) (Wing and Halevy, 2014). However, although the requirement for large fractionations at low csSRR constrains the electron carriers (and hence the metabolic pathway) under these conditions, it is possible that a shift in metabolic strategy occurs when favorable growth conditions allow a significant increase in csSRR. In fact, such a shift is consistent with the observed high csSRR in culture experiments and the correspondingly low S isotope fractionations. A switch in metabolic strategy could involve sulfur cycling through a separate enzymatic pathway, or a shift from strongly negative electron carriers in high-energy environments to modestly negative ones in low-energy environments. The latter switch could be implemented by different ratios of, for example, MK and Fd feeding into DSR, possibly through the involvement of separate transmembrane complexes (for example, Hmc or Tmc) that may be capable of receiving electrons from various donors.

Conclusions and implications

Living in low-energy environments is challenging. This is why the seemingly wasteful production of rubredoxin- and rubrerythrin-encoding gene transcripts in anoxic environments is puzzling (Lau *et al.*, 2016; Orsi *et al.*, 2016), given their assumed role as oxidative stress mitigators (Lumppio *et al.*, 2001). Using a systems biochemical-isotopic approach to address this apparent ecological inconsistency, we found that DSR can occur at low csSRR in these environments only with electron carriers with modestly negative reduction potentials like rubredoxin and rubrerythrin. It may be that these low-energy environments are transiently oxygenated (Contreras *et al.*, 2013), requiring constitutive maintenance of an oxygen defense system. In this case, low-potential proteins like rubredoxin and rubrerythrin may have been spandrelled into service as the electron carriers for DSR. Such functional co-option may be consistent with the view that evolution in energy-limited environments is essentially a sorting process rather than an adaptive one (Starnawski *et al.*, 2017). However, from a thermodynamic perspective, bacterial growth is most efficient when the energetic requirements for biomass synthesis and maintenance of cellular functions are balanced by energy production from the respiring processes (von Stockar *et al.*, 2006). This suggests that there may be a clear adaptive advantage to using electron carriers with modestly negative reduction potential in energy-limited environments.

In fact, when the net ΔG of the DSR pathway is compared among different electron carriers at the same csSRR (Supplementary Figure S2), our results show that electron carriers with modestly negative reduction potential require less available energy than high-potential carriers to maintain equivalent respiration rates. We suggest this is because less of the limited available energy is diverted toward inefficient redox reactions aimed at maintaining an available pool of high potential electron donors. In other words, as ATP production is proportional to the total rate of respiration (here sulfate reduction), electron carriers with modestly negative reduction potential allow production of enough ATP for survival at a smaller environmental ΔG (that is, more energy-limited conditions) than do strongly negative reduction potential electron carriers. As the difference in net ΔG is many orders of magnitude (Supplementary Figure S2), it seems possible that adoption of low-potential electron carriers may represent an adaptive solution to such a strong energetic selection pressure. Although here we specifically revealed physiological adaptations of SROs to energy-limited habitats, our approach can also be extended to study other metabolic pathways, such as sulfide oxidation, methanogenesis or anaerobic ammonium oxidation, through their natural variations in stable isotope fractionation.

Conflict of Interest

The authors declare no conflict of interest.

Acknowledgements

This study was initiated with the support of the Feinberg Foundation Visiting Faculty Program at the Weizmann Institute of Science. CBW acknowledges support from the Swiss Society of Friends of the Weizmann Institute of Science for a postdoctoral fellowship. IH acknowledges funding from a European Research Council Starting Grant 337183 and from an Israeli Science Foundation Grant 1133/12. BAW acknowledges support from a National Science and Engineering Research Council of Canada Discovery grant (RGPIN-2014-06626). We thank Ron Milo and Dan Tawfik for discussions and five anonymous reviewers for valuable comments on an earlier version of this manuscript.

References

Beard DA, Qian H. (2007). Relationship between thermodynamic driving force and one-way fluxes in reversible processes. *PLoS ONE* **2**: 4.

Bell GR, LeGall J, Peck HD. (1974). Evidence for periplasmic location of hydrogenase in *Desulfovibrio gigas*. *J Bacteriol* **120**: 994–997.

Bigeleisen J, Mayer MG. (1947). Calculation of equilibrium constants for isotopic exchange reactions. *J Chem Phys* **15**: 261–267.

Böttcher ME, Hespenheide B, Llobet-Brossa E, Beardsley C, Larsen O, Schramm A *et al.* (2000). The biogeochemistry, stable isotope geochemistry, and microbial community structure of a temperate intertidal mudflat: an integrated study. *Cont Shelf Res* **20**: 1749–1769.

Böttcher ME, Khim BK, Suzuki A, Gehre M, Wortmann UG, Brumsack H-J. (2004). Microbial sulfate reduction in deep sediments of the Southwest Pacific (ODP Leg 181, Sites 1119-1125): evidence from stable sulfur isotope fractionation and pore water modeling. *Marine Geol* **205**: 249–260.

Bowles MW, Mogollón JM, Kasten S, Zabel M, Hinrichs K-U. (2014). Global rates of marine sulfate reduction and implications for sub–sea-floor metabolic activities. *Science* **344**: 889–891.

Bradley AS, Leavitt WD, Johnston DT. (2011). Revisiting the dissimilatory sulfate reduction pathway. *Geobiology* **9**: 446–457.

Bradley AS, Leavitt WD, Schmidt M, Knoll AH, Girguis PR, Johnston DT. (2016). Patterns of sulfur isotope fractionation during microbial sulfate reduction. *Geobiology* **14**: 91–101.

Bruchert V, Knoblauch C, Jørgensen BB. (2001). Controls on stable sulfur isotope fractionation during bacterial sulfate reduction in Arctic sediments. *Geochim Cosmochim Acta* **65**: 763–776.

Brunner B, Bernasconi SM. (2005). A revised isotope fractionation model for dissimilatory sulfate reduction in sulfate reducing bacteria. *Geochim Cosmochim Acta* **69**: 4759–4771.

Canfield DE. (2001). Isotope fractionation by natural populations of sulfate-reducing bacteria. *Geochim Cosmochim Acta* **65**: 1117–1124.

Chambers LA, Trudinger PA, Smith JW, Burns MS. (1975). Fractionation of sulfur isotopes by continuous cultures of *Desulfovibrio desulfuricans*. *Can J Microbiol* **21**: 1602–1607.

Collins MD, Widdel F. (1986). Respiratory quinones of sulfate-reducing and sulfur-reducing bacteria - A systematic investigation. *Syst Appl Microbiol* **8**: 8–18.

Contreras S, Meister P, Liu B, Prieto-Mollar X, Hinrichs K-U, Khalili A *et al.* (2013). Cyclic 100-ka (glacial-interglacial) migration of subseafloor redox zonation on the Peruvian shelf. *Proc Natl Acad Sci USA* **110**: 18098–18103.

deMaré F, Kurtz DM, Nordlund P. (1996). The structure of *Desulfovibrio vulgaris* rubrerythrin reveals a unique combination of rubredoxin-like FeS4 and ferritin-like diiron domains. *Nat Struct Biol* **3**: 539–546.

Dörries M, Wöhlbrand L, Kube M, Reinhardt R, Rabus R. (2016). Genome and catabolic subproteomes of the marine, nutritionally versatile, sulfate-reducing bacterium *Desulfococcus multivorans* DSM 2059. *BMC Genomics* **17**: 918.

Duarte AG, Santos AA, Pereira IAC. (2016). Electron transfer between the QmoABC membrane complex and adenosine 5′-phosphosulfate reductase. *Biochim Biophys Acta* **1857**: 380–386.

Edwards KJ, Bach W, McCollom TM. (2005). Geomicrobiology in oceanography: microbe–mineral interactions at and below the seafloor. *Trends Microbiol* **13**: 449–456.

Eldridge DL, Guo W, Farquhar J. (2016). Theoretical estimates of equilibrium sulfur isotope effects in aqueous sulfur systems: highlighting the role of isomers in the sulfite and sulfoxylate systems. *Geochim Cosmochim Acta* **195**: 171–200.

Fauque G, Peck HD, Moura JJG, Huynh BH, Berlier Y, DerVartanian DV *et al.* (1988). The three classes of hydrogenases from sulfate-reducing bacteria of the genus *Desulfovibrio*. *FEMS Microbiol Revi* **4**: 299–344.

Flamholz A, Noor E, Bar-Even A, Liebermeister W, Milo R. (2013). Glycolytic strategy as a tradeoff between energy yield and protein cost. *Proc Natl Acad Sci USA* **110**: 10039–10044.

Fritz G, Büchert T, Kroneck PMH. (2002). The function of the 4Fe-4S clusters and FAD in bacterial and archaeal adenylylsulfate reductases - evidence for flavin-catalyzed reduction of adenosine 5 ′-phosphosulfate. *J Biol Chem* **277**: 26066–26073.

Goldhaber MB, Kaplan IR. (1975). Controls and consequences of sulfate reduction rates in recent marine sediments. *Soil Sci* **119**: 42–55.

Grein F, Ramos AR, Venceslau SS, Pereira IAC. (2013). Unifying concepts in anaerobic respiration: insights from dissimilatory sulfur metabolism. *Biochim Biophys Acta* **1827**: 145–160.

Habicht KS, Canfield DE. (2001). Isotope fractionation by sulfate-reducing natural populations and the isotopic composition of sulfide in marine sediments. *Geology* **29**: 555–558.

Habicht KS, Salling L, Thamdrup B, Canfield DE. (2005). Effect of low sulfate concentrations on lactate oxidation and isotope fractionation during sulfate reduction by *Archaeoglobus fulgidus* strain Z. *Appl Environ Microbiol* **71**: 3770–3777.

Harrison AG, Thode HG. (1958). Mechanism of the bacterial reduction of sulphate from isotope fractionation studies. *Transact Faraday Soc* **54**: 84–92.

Hocking WP, Stokke R, Roalkvam I, Steen IH. (2014). Identification of key components in the energy metabolism of the hyperthermophilic sulfate-reducing archaeon *Archaeoglobus fulgidus* by transcriptome analyses. *Front Microbiol* **5**: 20.

Hoehler TM, Jørgensen BB. (2013). Microbial life under extreme energy limitation. *Nat Rev Microbiol* **11**: 83–94.

Ivanov MV, Rusanov II, Pimenov NV, Bairamov IT, Yusupov SK, Savvichev AS *et al.* (2001). Microbial processes of the carbon and sulfur cycles in Lake Mogil'noe. *Microbiology* **70**: 583–593.

Johnston DT, Farquhar J, Canfield DE. (2007). Sulfur isotope insights into microbial sulfate reduction: when microbes meet models. *Geochim Cosmochim Acta* **71**: 3929–3947.

Jørgensen BB. (1982). Mineralization of organic matter in the sea bed - the role of sulphate reduction. *Nature* **296**: 643–645.

Jørgensen BB, D'Hondt S. (2006). A starving majority deep beneath the seafloor. *Science* **314**: 932–934.

Jørgensen BB, Marshall IPG. (2016). Slow microbial life in the seabed. *Ann Rev Mar Sci* **8**: 311–332.

Kallmeyer J, Pockalny R, Adhikari RR, Smith DC, D'Hondt S. (2012). Global distribution of microbial abundance and biomass in subseafloor sediment. *Proc Natl Acad Sci USA* **109**: 16213–16216.

Kaplan IR, Emery KO, Rittenberg SC. (1963). The distribution and isotopic abundance of sulphur in recent marine sediments off Southern California. *Geochim Cosmochim Acta* **27**: 297–312.

Kaplan IR, Rittenberg SC. (1964). Microbiological fractionation of sulphur isotopes. *J Gen Microbiol* **34**: 195–212.

Keller AH, Schleinitz KM, Starke R, Bertilsson S, Vogt C, Kleinsteuber S. (2015). Metagenome-based metabolic reconstruction reveals the ecophysiological function of *Epsilonproteobacteria* in a hydrocarbon-contaminated sulfidic aquifer. *Front Microbiol* **6**: 1396.

Keller KL, Wall JD. (2011). Genetics and molecular biology of the electron flow for sulfate respiration in *Desulfovibrio*. *Front Microbiol* **2**: 17.

Keller KL, Rapp-Giles BJ, Semkiw ES, Porat I, Brown SD, Wall JD. (2014). New model for electron flow for sulfate reduction in *Desulfovibrio alaskensis* G20. *Appl Environ Microbiol* **80**: 855–868.

Kemp ALW, Thode HG. (1968). The mechanism of bacterial reduction of sulphate and of sulphite from isotope fractionation studies. *Geochim Cosmochim Acta* **32**: 71–91.

Kremer DR, Nienhuiskuiper HE, Hansen TA. (1988). Ethanol dissimilation in *Desulfovibrio*. *Arch Microbiol* **150**: 552–557.

Lau MCY, Kieft TL, Kuloyo O, Linage-Alvarez B, Van Heerden E, Lindsay MR *et al.* (2016). An oligotrophic deep-subsurface community dependent on syntrophy is dominated by sulfur-driven autotrophic denitrifiers. *Proc Natl Acad Sci USA* **113**: E7927–E7936.

Leavitt WD, Halevy I, Bradley AS, Johnston DT. (2013). Influence of sulfate reduction rates on the Phanerozoic sulfur isotope record. *Proc Natl Acad Sci USA* **110**: 11244–11249.

Leavitt WD, Bradley AS, Santos AA, Pereira AS, Johnston DT. (2015). Sulfur isotope effects of dissimilatory sulfite reductase. *Front Microbiol* **6**: 1392.

LeGall J. (1968). Purification partielle et étude de la NAD: rubrédoxin oxydo-réductase de *D. gigas*. *Annal Inst Pasteur* **114**: 109–115.

LeGall J, Peck HD. (1987). Amino-terminal amino-acid-sequences of electron-transfer proteins from gram-negative bacteria as indicators of their cellular-localization - the sulfate-reducing bacteria. *FEMS Microbiol Lett* **46**: 35–40.

LeGall J, Prickril BC, Moura I, Xavier AV, Moura JJG, Huynh BH. (1988). Isolation and characterization of rubrerythrin, a non-heme iron protein from *Desulfovibrio vulgaris* that contains rubredoxin centers and a hemerythrin-like binuclear iron cluster. *Biochemistry* **27**: 1636–1642.

Lever MA, Rogers KL, Lloyd KG, Overmann J, Schink B, Thauer RK *et al.* (2015). Life under extreme energy limitation: a synthesis of laboratory- and field-based investigations. *FEMS Microbiol Rev* **39**: 688–728.

Lumppio HL, Shenvi NV, Summers AO, Voordouw G, Kurtz DM. (2001). Rubrerythrin and rubredoxin oxidoreductase in *Desulfovibrio vulgaris*: a novel oxidative stress protection system. *J Bacteriol* **183**: 101–108.

Milo R, Phillips R. (2015). *Cell Biology by the Numbers*. Garland Science, Taylor & Francis Group, LLC: New Yok, NY, USA.

Moura I, Pereira AS, Tavares P, Moura JJG. (1999). Simple and complex iron-sulfur proteins in sulfate reducing bacteria. *Adv Inorg Chem*. **47**: 361–419.

Oberding L, Gieg LM. (2016). Metagenomic analyses reveal that energy transfer gene abundances can predict the syntrophic potential of environmental microbial communities. *Microorganisms* **4**: 5.

Odom JM, Bruschi M, Peck HD, LeGall J. (1976). Structure-function-relationships among rubredoxins - comparative reactivities with NADH - rubredoxin oxidoreductase from *Desulfovibrio gigas*. *Fed Proc* **35**: 1360–1360.

Odom JM, Peck HD. (1984). Hydrogenase, electron-transfer proteins, and energy coupling in the sulfate-reducing bacteria *Desulfovibrio*. *Annu Rev Microbiol* **38**: 551–592.

Ogata M, Yagi T. (1986). Pyruvate dehydrogenase and the path of lactate degradation in *Desulfovibrio vulgaris* Miyazaki F. *J Biochem* **100**: 311–318.

Oliveira TF, Vonrhein C, Matias PM, Venceslau SS, Pereira IAC, Archer M. (2008). The crystal structure of *Desulfovibrio vulgaris* dissimilatory sulfite reductase bound to DsrC provides novel insights into the mechanism of sulfate respiration. *J Biol Chem* **283**: 34141–34149.

Orsi WD, Edgcomb VP, Christman GD, Biddle JF. (2013). Gene expression in the deep biosphere. *Nature* **499**: 205–208.

Orsi WD, Jørgensen BB, Biddle JF. (2016). Transcriptional analysis of sulfate reducing and chemolithoautotrophic sulfur oxidizing bacteria in the deep subseafloor. *Environ Microbiol Rep* **8**: 452–460.

Otake T, Lasaga AC, Ohmoto H. (2008). Ab initio calculations for equilibrium fractionations in multiple sulfur isotope systems. *Chem Geol* **249**: 357–376.

Pereira IAC, Ramos AR, Grein F, Marques MC, da Silva SM, Venceslau SS. (2011). A comparative genomic analysis of energy metabolism in sulfate reducing bacteria and archaea. *Front Microbiol* **2**: 22.

Pires RH, Lourenço AI, Morais F, Teixeira M, Xavier AV, Saraiva LgM *et al.* (2003). A novel membrane-bound respiratory complex from *Desulfovibrio desulfuricans* ATCC 27774. *Biochim Biophys Acta* **1605**: 67–82.

Price MN, Ray J, Wetmore KM, Kuehl JV, Bauer S, Deutschbauer AM. (2014a). The genetic basis of energy conservation in the sulfate-reducing bacterium *Desulfovibrio alaskensis* G20. *Front Microbiol* **5**: 577.

Price MN, Ray J, Wetmore KM, Kuehl JV, Bauer S, Deutschbauer AM *et al.* (2014b). The genetic basis of energy conservation in the sulfate-reducing bacterium *Desulfovibrio alaskensis* G20. *Front Microbiol* **5**: 577.

Rabus R, Hansen TA, Widdel F. (2006). *Dissimilatory Sulfate- and Sulfur-Reducing Prokaryotes*. Springer: New York, NY, USA.

Rabus R, Hansen TA, Widdel F. (2013). *Dissimilatory Sulfate- and Sulfur-Reducing Prokaryotes*. Springer-Verlag: Berlin Heidelberg.

Rabus R, Venceslau SS, Wöhlbrand L, Voordouw G, Wall JD, Pereira IAC. (2015). Chapter two - a post-genomic view of the ecophysiology, catabolism and biotechnological relevance of sulphate-reducing prokaryotes. *Adv Microb Physiol* **66**: 55–321.

Ramos AR, Keller KL, Wall JD, Pereira IAC. (2012). The membrane QmoABC complex interacts directly with the dissimilatory adenosine 5'-phosphosulfate reductase in sulfate reducing bacteria. *Front Microbiol* **3**: 10.

Rees CE. (1973). Steady-state model for sulfur isotope fractionation in bacterial reduction processes. *Geochim Cosmochim Acta* **37**: 1141–1162.

Santos AA, Venceslau SS, Grein F, Leavitt WD, Dahl C, Johnston DT *et al.* (2015). A protein trisulfide couples dissimilatory sulfate reduction to energy conservation. *Science* **350**: 1541–1545.

Sim MS, Bosak T, Ono S. (2011a). Large sulfur isotope fractionation does not require disproportionation. *Science* **333**: 74–77.

Sim MS, Ono S, Donovan K, Templer SP, Bosak T. (2011b). Effect of electron donors on the fractionation of sulfur isotopes by a marine *Desulfovibrio* sp. *Geochim Cosmochim Acta* **75**: 4244–4259.

Sim MS, Ono S, Bosak T. (2012). Effects of iron and nitrogen limitation on sulfur isotope fractionation during microbial sulfate reduction. *Appl Environ Microbiol* **78**: 8368–8376.

Starnawski P, Bataillon T, Ettema TJG, Jochum LM, Schreiber L, Chen X *et al.* (2017). Microbial community assembly and evolution in subseafloor sediment. *Proc Natl Acad Sci USA* **114**: 2940–2945.

Thauer RK, Jungermann K, Decker K. (1977). Energy conservation in chemotrophic anaerobic bacteria. *Bacteriol Rev* **41**: 100–180.

Tindall BJ, Stetter KO, Collins MD. (1989). A novel, fully saturated menaquinone from the thermophilic, sulfate-reducing archaebacterium *Archaeoglobus fulgidus*. *J Gen Microbiol* **135**: 693–696.

Urey HC. (1947). The thermodynamic properties of isotopic substances. *J Chem Soc*, 562–581.

Venceslau SS, Lino RR, Pereira IAC. (2010). The Qrc membrane complex, related to the alternative complex III, is a menaquinone reductase involved in sulfate respiration. *J Biol Chem* **285**: 22774–22783.

Venceslau SS, Stockdreher Y, Dahl C, Pereira IAC. (2014). The "bacterial heterodisulfide" DsrC is a key protein in dissimilatory sulfur metabolism. *Biochim Biophys Acta* **1837**: 1148–1164.

von Stockar U, Maskow T, Liu J, Marison IW, Patiño R. (2006). Thermodynamics of microbial growth and metabolism: an analysis of the current situation. *J Biotechnol* **121**: 517–533.

Werne JP, Lyons TW, Hollander DJ, Formolo MJ, Damsté JSS. (2003). Reduced sulfur in euxinic sediments of the Cariaco Basin: sulfur isotope constraints on organic sulfur formation. *Chem. Geol* **195**: 159–179.

Whitman WB, Coleman DC, Wiebe WJ. (1998). Prokaryotes: The unseen majority. *Proc Natl Acad Sci USA* **95**: 6578–6583.

Wing BA, Halevy I. (2014). Intracellular metabolite levels shape sulfur isotope fractionation during microbial sulfate respiration. *Proc Natl Acad Sci USA* **111**: 18116–18125.

Wortmann UG, Bernasconi SM, Böttcher ME. (2001). Hypersulfidic deep biosphere indicates extreme sulfur isotope fractionation during single-step microbial sulfate reduction. *Geology* **29**: 647–650.

Wu X, Holmfeldt K, Hubalek V, Lundin D, Astrom M, Bertilsson S *et al.* (2016). Microbial metagenomes from three aquifers in the Fennoscandian shield terrestrial deep biosphere reveal metabolic partitioning among populations. *ISME J* **10**: 1192–1203.

Zhou J, He Q, Hemme CL, Mukhopadhyay A, Hillesland K, Zhou A *et al.* (2011). How sulphate-reducing microorganisms cope with stress: lessons from systems biology. *Nat Rev Microbiol* **9**: 452–466.

Supplementary Information accompanies this paper on The ISME Journal website (http://www.nature.com/ismej)